Mod Pathol 37 (2024) 100558

MODERN PATHOLOGY

USCAP UNITED STATES AND CANADIAN ACADEMY OF PATHOLOGY
Creating a Better Pathologist

Journal homepage: https://modernpathology.org/

Research Article

Immune Phenotype-Genotype Associations in Primary Clear Cell Renal Cell Carcinoma and Matched Metastatic Tissue

Bettina Sobottka[a,*], Viola Vetter[a], Amir Banaei-Esfahani[a], Marta Nowak[a], Anja Lorch[b], Andrej Sirek[c], Kirsten D. Mertz[c,d], Matteo Brunelli[e], Dominik Berthold[f], Laurence de Leval[g], Abdullah Kahraman[a,h,i], Viktor Hendrik Koelzer[a,d], Holger Moch[a]

[a] *Department of Pathology and Molecular Pathology, University Hospital Zurich, University of Zurich, Zurich, Switzerland;* [b] *Department of Medical Oncology and Hematology, University Hospital Zurich, Zurich, Switzerland;* [c] *Institute of Pathology, Cantonal Hospital Baselland, Liestal, Switzerland;* [d] *Institute of Medical Genetics and Pathology, University Hospital of Basel, Basel, Switzerland;* [e] *Università di Verona, Azienda Ospedaliera Universitaria Integrata di Verona, Verona, Italy;* [f] *Department of Oncology, Lausanne University Hospital and Lausanne University, Lausanne, Switzerland;* [g] *Institute of Pathology, Department of Laboratory Medicine and Pathology, Lausanne University Hospital and Lausanne University, Lausanne, Switzerland;* [h] *Swiss Institute of Bioinformatics, Lausanne, Switzerland;* [i] *School of Life Sciences Fachhochschule Nordwestschweiz, Institute for Chemistry and Bioanalytics, Muttenz, Switzerland*

ARTICLE INFO

Article history:
Received 23 October 2023
Revised 11 June 2024
Accepted 26 June 2024
Available online 4 July 2024

Keywords:
CD8+ T cells
clear cell renal cell carcinoma
immune phenotype
metastasis
genotype

ABSTRACT

Adjuvant immunotherapy has been recently recommended for patients with metastatic clear cell renal cell carcinoma (ccRCC), but there are no tissue biomarkers to predict treatment response in ccRCC. Potential predictive biomarkers are mainly assessed in primary tumor tissue, whereas metastases (METs) remain understudied. To explore potential differences between genomic alterations and immune phenotypes in primary tumors and their matched METs, we analyzed primary tumors (PTs) of 47 ccRCC patients and their matched distant METs by comprehensive targeted parallel sequencing, whole-genome copy number variation analysis, determination of microsatellite instability, and tumor mutational burden. We quantified the spatial distribution of tumor-infiltrating $CD8^+$ T cells and coexpression of the T-cell-exhaustion marker thymocyte selection-associated high mobility group box (TOX) by digital immunoprofiling and quantified tertiary lymphoid structures. Most METs were pathologically "cold." Inflamed, pathologically "hot" PTs were associated with decreased disease-free survival, worst for patients with high levels of $CD8^+TOX^+$ T cells. Interestingly, inflamed METs showed a relative increase in exhausted $CD8^+TOX^+$ T cells and increased accumulative size of tertiary lymphoid structures compared with PTs. Integrative analysis of molecular and immune phenotypes revealed *BAP1* and *CDKN2A/B* deficiency to be associated with an inflamed immune phenotype. Our results highlight the distinct spatial distribution and differentiation of CD8+ T cells at metastatic sites, and the association of an inflamed microenvironment with specific genomic alterations.

Introduction

One-third of clear cell renal cell carcinoma (ccRCC) patients present with synchronous metastases, and another third will develop metachronous metastases over the course of disease.[1]

* Corresponding author.
E-mail address: annabettina.sobottka-brillout@usz.ch (B. Sobottka).

https://doi.org/10.1016/j.modpat.2024.100558

Therapeutic advances, especially vascular endothelial growth factor-targeted therapy or immune checkpoint inhibitors (ICIs), have improved the prognosis of many advanced ccRCC patients.[2-4] Yet, a significant number of patients with metastatic ccRCC do not profit from immunotherapy potentially due to differences within the tumor immune microenvironment (TIME).[5]

While inactivation of *VHL* through various mechanisms[6] is essential for ccRCC tumor initiation, genetic alterations in additional other tumor suppressor genes, like loss of *BAP1* or *PBRM1*,[7] seem necessary for tumor progression. Recently, it was shown that some tumor suppressor genes are associated with tumor inflammation or response to ICI:*BAP1* deficiency is associated with high-grade ccRCC, poor outcome,[7-9] tumor inflammation,[10] increased PD-L1 expression, a T effector cell signature, and good response to ICI.[11] Conversely, *PBRM1*-deficient ccRCC display a rather well-differentiated, prototypic morphology in humans and mice[12] with improved clinical outcome and reduced inflammation.[11,13] *PBRM1*-mutated ccRCC frequently carries additional mutations in *SETD2*, which seem to occur after *PBRM1* mutations within the same tumor.[14] *SETD2* mutations increase in frequency upon disease progression, implicating a function in preventing metastasis.[15] These data highlight the importance of an integrated characterization of genomic features and immunologic characteristics of primary ccRCC for accurate patient stratification.

Studies investigating the immune cell composition mostly focused on primary ccRCC,[16-20] nonmatched metastases[21,22] or examined only very few primary tumors and their matched metastases.[23] Methods were limited to hematoxylin and eosin, mostly single-stain immunohistochemistry at broad scale or bioinformatic deconvolution from gene expression signatures.[24,25] Despite the importance for therapeutic stratification, the spatial distribution and amount of immune cells within the tumor compartments, particularly of tumor-infiltrating $CD8^+$ T cells, were not assessed. Standardized and reproducible evaluations are also lacking. Yet, dysfunctional or exhausted $CD8^+$ T cells represent the main clinical target in ICI therapy.[26] Their distribution pattern within the tumor compartments correlates with response to ICI in many malignancies,[27] referred to as inflamed or pathologically "hot," and immune excluded or desert tumors, pathologically "cold."[28] For increased reproducibility, we recently established standardized immune phenotyping of metastatic melanoma using digital pathology[29] and have described the application to immunotherapy-treated ccRCC as well as other cancer types.[30,31]

The objective of this study was to identify potential differences in the genetic landscape and immune cell infiltration between PT and their corresponding metastases (METs). The underlying causes of why METs frequently exhibit diminished inflammatory infiltration are presently not well understood, particularly in the context of ccRCC. It has been hypothesized that somatic alterations could influence immune cell infiltration. Therefore, we investigated 47 ccRCC PTs and their METs. We combined different molecular and histologic methods such as comprehensive targeted parallel sequencing, whole-genome copy number variation analysis, determination of microsatellite instability and tumor mutational burden, spatially resolved digital immunoprofiling, and digital quantification and morphometry of tertiary lymphoid structures. Further, we included TOX, a marker described to positively correlate with expression of PD1 and other markers of T-cell exhaustion in human cancer[32] and frequently expressed by exhausted and polyfunctional effector memory CD8+ T cells. Although TOX is not directly targeted by immune checkpoint immunotherapy, it can be regarded as a predictor of anti-PD1 treatment response in several malignancies,[32,33] and TOX expression may reflect truly terminally exhausted T cells in contrast to established exhaustion markers like PD1, PD-L1.[34] In our cohort, increased CD8+ T cells within PTs correlated with an overall decreased disease-free survival (DFS). Interestingly, although the total number of tumor-infiltrating $CD8^+$ T cells remained similar in inflamed METs compared with their matched PTs, we observed a relative increase in TOX^+ expression, potentially indicating increased levels of $CD8^+$ T-cell exhaustion. Loss of *BAP1* and *CDKN2A/B* was associated with an inflamed immune phenotype both in PTs and METs. Our data suggest that conducting a combined analysis of comprehensive molecular genotyping alongside spatially resolved tissue immune phenotyping, preferably within METs, could be clinically most informative for advanced ccRCC patients.

Materials and Methods

Patient Cohort

We collected treatment-naïve PTs of 47 ccRCC patients and their matched distant metastases (METs) from different anatomical locations. The majority of cases were retrieved from the archives of the Department of Pathology and Molecular Pathology, University Hospital Zurich, Switzerland, between 2001 and 2020 ($n = 29$). Further cases from the Institute of Pathology, Cantonal Hospital Baselland, Liestal, Switzerland ($n = 5$); the Department of Pathology and Diagnostics, University of Verona, Italy ($n = 5$); and the Institute of Pathology, Department of Laboratory Medicine and Pathology, Lausanne, Switzerland ($n = 8$), were included, the latter as part of the Swiss Patholink consortium. All cases were reviewed by 2 expert pathologists (B.S. and H.M.). Selection criteria included a histologic and immunohistochemical phenotype consistent with ccRCC in both the primary tumor and matched distant metastasis. Distant metastases had occurred to lung ($n = 10$), bone ($n = 8$), brain ($n = 9$), pancreas ($n = 7$) or soft tissue, adrenal gland, pleura, or stomach ($n = 20$), the latter summarized as "other," and for 7 patients, an additional longitudinal metastasis sample was available (patient IDs: 5, 12, 14, 33, 34, 40, and 43), resulting in a total of 54 metastatic samples (Table 1). Metastatic tissue consisted of excision specimens ($n = 37$; 68.5%), open biopsies/currettings ($n = 14$; 30%), and very few core needle biopsies ($n = 3$; 5.5%). Clinical data including clinical stage, treatment, clinical progression-free survival assessed by imaging, and overall survival could be retrieved for the majority of patients ($n = 43$). All 47 patients had undergone surgical treatment of their primary ccRCC (partial or complete nephrectomy). The majority received adjuvant treatment ($n = 30$ patients), and only 13 patients were treated by surgery only. Of the 54 metastatic samples, 31 metastases were treatment-naïve, 7 metastases were pretreated with ICI and systemic therapy (TKI) (sample IDs: 24, 27, 33, 35, 36, 37, and 44), 1 metastasis with ICI only (sample ID: 16), 14 metastases had been treated with systemic therapy (TKI) but not ICI, and for 1 sample, pretreatment data of the metastasis were not available (Fig. 1).

Nucleic Acid Extraction

DNA was extracted from microdissected or punched formalin-fixed paraffin-embedded tumor tissues using the RecoverAll Total Nucleic Acid Isolation Kit (Cat No. AM1975, ThermoFisher Scientific) according to the diagnostic accredited guidelines. Sampling included multiple regions from the tumor center to capture intratumoral heterogeneity and avoid the potential discovery of

Table 1
Clinicopathological information of the study cohort

ccRCC Cohort	Site of metastatic biopsy ($n = 54$)				
Characteristics ($n = 47$)	Lung	Bone	Brain	Pancreas	Other
Patient characteristics					
Age at initial diagnosis <60	4	4	5	4	3
Age at initial diagnosis ≥60	6	4	4	3	17
Female	3	2	3	3	6
Male	7	6	6	4	14
Clinical stage 1	3	3	2	3	2
Clinical stage 2	0	1	3	0	2
Clinical stage 3	6	1	1	0	9
Clinical stage 4	1	3	3	4	7
Disease characteristics					
Tumor (pT) stage					
pT1a	0	2	0	1	3
pT1b	2	2	2	2	1
pT2a	0	0	0	1	0
pT2b	0	1	3	0	2
pT3a	5	2	4	2	12
pT3b	3	1	0	1	1
pT4a	0	0	0	0	1
Fuhrman grade					
Grade 1	0	0	0	1	2
Grade 2	4	3	1	0	5
Grade 3	3	3	6	6	10
Grade 4	3	2	2	0	3
Treatment characteristics					
Surgery only	3	3	1	1	7
Radiotherapy	6	3	6	1	3
Systemic treatment (TKI)	3	5	4	1	12
ICI	5	1	2	0	2
Not available	0	0	0	4	0
Metastatic biopsy characteristics					
Treatment naïve	7	3	6	6	9
Prior treatment	4	5	3	0	10
Not available	0	0	0	1	0

Detailed clinicopathological information including treatment is provided. Only primary tumors from ccRCC patients were included and are grouped according to their site of distant metastases.
ccRCC, clear cell renal cell carcinoma; ICI, immune checkpoint inhibitor.

clonal genetic alterations.[35] Samples used for genetic profiling were taken from the same blocks as the samples used for histologic studies. Nucleic acid concentrations were measured with Qubit dsDNA HS and RNA HS Assay Kits (Cat No. Q32851 and Q32852, ThermoFisher Scientific).

Next-Generation Sequencing

Next-generation sequencing (NGS) library preparation and bioinformatics analysis were conducted according to diagnostic-approved standards. All shown samples passed the internal quality criteria including DNA quality, mean coverage, mapped reads, and read lengths. In detail, we performed targeted parallel sequencing of genomic DNA using the FoundationOne CDx comprehensive genomic profiling assay. This panel covers the exonic regions of 324 disease-relevant genes as well as selected intronic regions of 36 genes, which are frequently involved in fusion events. Genomic biomarkers, including tumor mutational burden, microsatellite instability, and loss-of-heterozygosity (LOH), were also assessed. Mutational data were retrieved from Foundation Medicine via One-Alteration-Per-Line Files and processed with custom R, PERL, and Bash scripts, which are available at https://github.com/mtp-usz/ccRCC_Primary-Metastases.

Genome-Wide Copy Number Analysis

For genome-wide copy number analysis, we subjected 500 ng genomic DNA from each sample to bisulfite conversion using the EZ DNA Methylation Kit (Cat. No. D5001, Zymo) according to the manufacturer's guidelines. The Infinium Human Methylation EPIC 850 k array was used to obtain genome-wide DNA methylation profiles from FFPE tumor samples, according to the manufacturer's instructions (Illumina). Data (IDAT files) were analyzed through the *minfi* R package. Copy number calculations on the IDAT files were performed using R (version 4.0.4) and the *conumee* Bioconductor[36] package (version 1.26.0). Prior to the calculations, IDAT files were imported to R using the *minfi*[37] Bioconductor

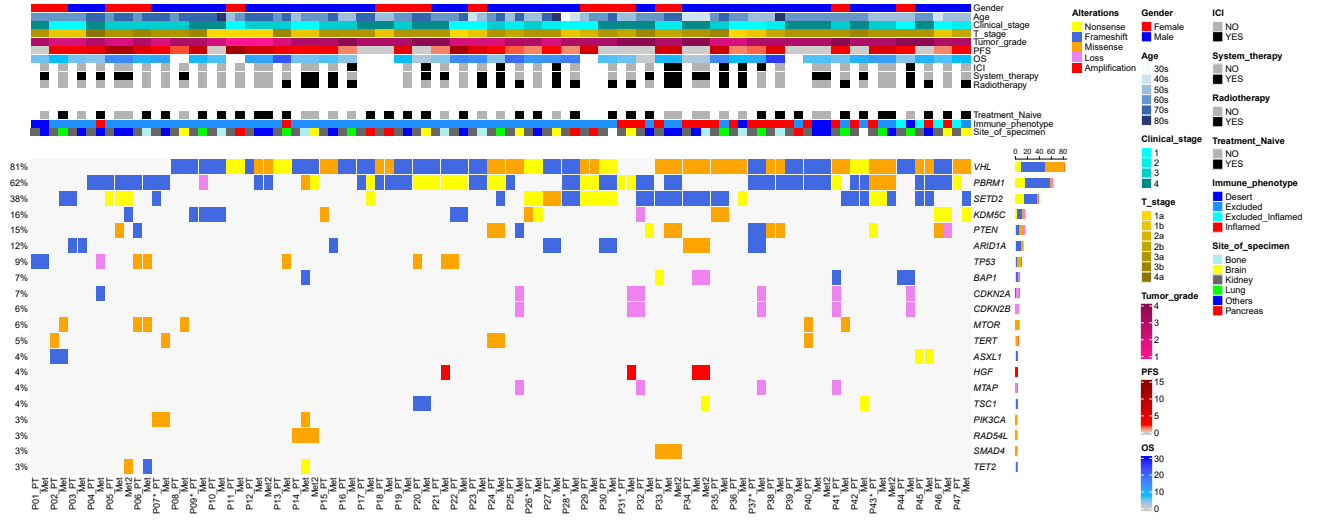

Figure 1.
Oncoprint visualization of the clinic-pathological parameters, the immune phenotypes and genomic findings. Clinical parameters such as sex, age, clinical stage, therapy after resection of the primary tumor, treatment naïveness of the metastatic biopsy, progression-free survival, overall survival, and immune phenotypes are depicted on a single patient level as indicated. Patient IDs indicated with an asterisk are patients alive at the time of publication. Each gene is depicted as a row, and each primary tumor and the matched METs as respective columns per patient.

package (v.1.36.0) and converted to *conumee* compatible MethylSet objects. The failed probes of the data set were identified as both the methylated and unmethylated channel reported background signal levels ($P > .01$). Probes that failed in more than 5% of the samples were removed. The data were then normalized using both Illumina and FunNorm methods for the downstream copy number variation and methylation analyses, respectively. Moreover, we performed differential methylated analysis on both probe and region levels using the methods implemented in the R package *minfi*.[37] Normalized probe intensities were subsequently clustered into segments using the circular binary segmentation algorithm with an acceptance significance level of $\alpha = 0.05$, 10,000 permutations, a minimum of 5 probes per segment, and without undoing change points. Copy number spectrum plots were generated using the cnSpec function in the *GenVisR* (86) Bioconductor package (version 1.22.1).

Immunohistochemistry

Immunohistochemical analysis was performed utilizing the monoclonal mouse anti-human CD8 (clone 4B11, Leica Biosystems), the monoclonal mouse-anti-human CD20 (clone L26, Roche Diagnostics), and the polyclonal rabbit-anti-human TOX (Cat No. PA5-30328, ThermoFisher Scientific) antibodies after tissue pretreatment according to the manufacturer's instructions. Antibody binding was visualized using either the OptiView (Roche Diagnostics) or Bond Polymer Refine Red Detection (Leica Biosystems) kits. Although all cases showed robust CD8 and CD20 staining, 6 PTs and 6 METs repeatedly showed a weak TOX staining signal and were excluded from the CD8/TOX costain analysis. One MET was excluded completely from immuhistochemical analysis because of technical reasons.

Digital Image Analysis, Immune Phenotypes, and Tertiary Lymphoid Structures Evaluation

Stained slides were digitalized on a 3DHistech P1000 digital slide scanner (3D Histech) at ×40 magnification and a resolution of 0.24 μm per pixel. Digital slide review, annotation of tumor regions as recommended by the International Immuno-Oncology Biomarker Working Group,[38] and quality controls were performed by an expert image analyst (V.V.) and reviewed by a board-certified pathologist (V.H.K.). We then created a virtual tissue microarray (vTMA), consisting of 5 spots each of the tumor center and the tumor invasive margin compartment. vTMAs are effective tools for high-throughput analysis of highly standardized tissue regions in histologically defined tumor microenvironment compartments.[39] The vTMA approach thus allows us to apply standardized selection rules (tumor center, invasive margin, and immune infiltration parameters) for the comparative analysis of immune cell infiltrates and biomarker expression analysis across large and heterogeneous sample sets while excluding areas of artefact by expert pathology review. vTMA spots were circular with a diameter of 600 μm and were placed in the regions with the highest diffuse infiltration of T cells. Regions containing tertiary lymphoid structures (TLS) were annotated separately and excluded from the evaluation of diffuse immune infiltrates. In cases with limited tissue availability, ($n = 5$ METs), a minimum of 3 vTMAs spots were placed. In one case, where placement of at least 3 spots was not possible, whole-slide analysis was performed. vTMAs for the invasive margin compartment were only created when the invasive margin was included in the scan.

Digital image analysis was performed using HALO (HALO v3-2-1851.266, Indica Lavbs) (Supplementary Table S1). For cell-level analysis, nuclear segmentation was performed with a pretrained nuclei segmentation algorithm (AI default) and optimized using cell-morphometric parameters. CD8+ and TOX+ marker-positive cells were quantified according to pathologist-set intensity thresholds for the membrane/cytoplasmic (CD8) and nuclear compartment (TOX). Unstained nonimmune tissue on the same slide served as internal control. $CD8^+TOX^+$, $CD8^+TOX^-$, and $CD8^-TOX^+$ cell counts were normalized by tissue area (mm^2) to determine infiltration density. We evaluated the spatial distribution of CD8+ T cells[38] by creating virtual TMAs approximating whole-slide analyses.[39]

TLS were identified by CD20 staining within the intra- and extratumoral compartment, where the extratumoral compartment was stringently defined by pathologist review to exclude adjacent normal tissue. TLS were defined as dense lymphocyte aggregates, containing clusters of $CD20^+$ B cells, with a minimum size of 15,000 μm^2. The boundary of each TLS was annotated based on evaluation of H&E-, CD20-, and CD8/TOX-stained serial sections, and the amount and area occupied by the TLS was individually measured.

Statistics

Statistical analysis was performed using GraphPad Prism (version 8.0.0) for Fisher exact tests, Wilcoxon tests, and 2-way analysis of variance with Tukey-Kramer posttest for multiple comparisons and unequal sample sizes.

Results

Exhausted $CD8^+TOX^+$ T Cells Are Relatively Increased at Matched Metastatic Sites

For immune phenotyping, 2 expert pathologists first categorized PTs and METs into the following immune diagnostic categories: immune desert, immune excluded, or inflamed, based on the overall spatial distribution of $CD8^+$ T cells[29,40] (Fig. 2; Supplementary Fig. S1). PTs showed either an excluded ($n = 29$; 61%) or inflamed ($n = 13$; 28%) immune phenotype; 1 PT (2%) was classified as desert. We also observed 2 distinct but adjacent immune infiltration patterns within a single PT in 4 cases (9%), which we termed "dual immune phenotype" (not shown) as recently described.[29]

Interestingly, the matched metastases predominantly showed a clinically "cold" immune phenotype (desert $n = 5$; 9% and excluded $n = 40$; 74%), irrespective of the site of metastasis (Fig. 3A), their time of occurrence (synchronous vs metachronous), or prior treatment with ICI (desert $n = 2$ and excluded $n = 4$). Among the inflamed metastases ($n = 9$; 16%), 1 had received prior ICI treatment, and the majority were associated with inflamed or excluded/inflamed primary tumors ($n = 6$; 66%). To evaluate the quantity and functional state of CD8/TOX T cells in PT and METs at single-cell resolution, digital image analysis was performed of CD8+ (red) and TOX+ (brown) T-cell infiltration in the tumor center and invasive margin compartments (Fig. 3B, C). As the presence of TLS in the TIME is seen as an enabler of naïve T-cell infiltration and intra-/peritumoral

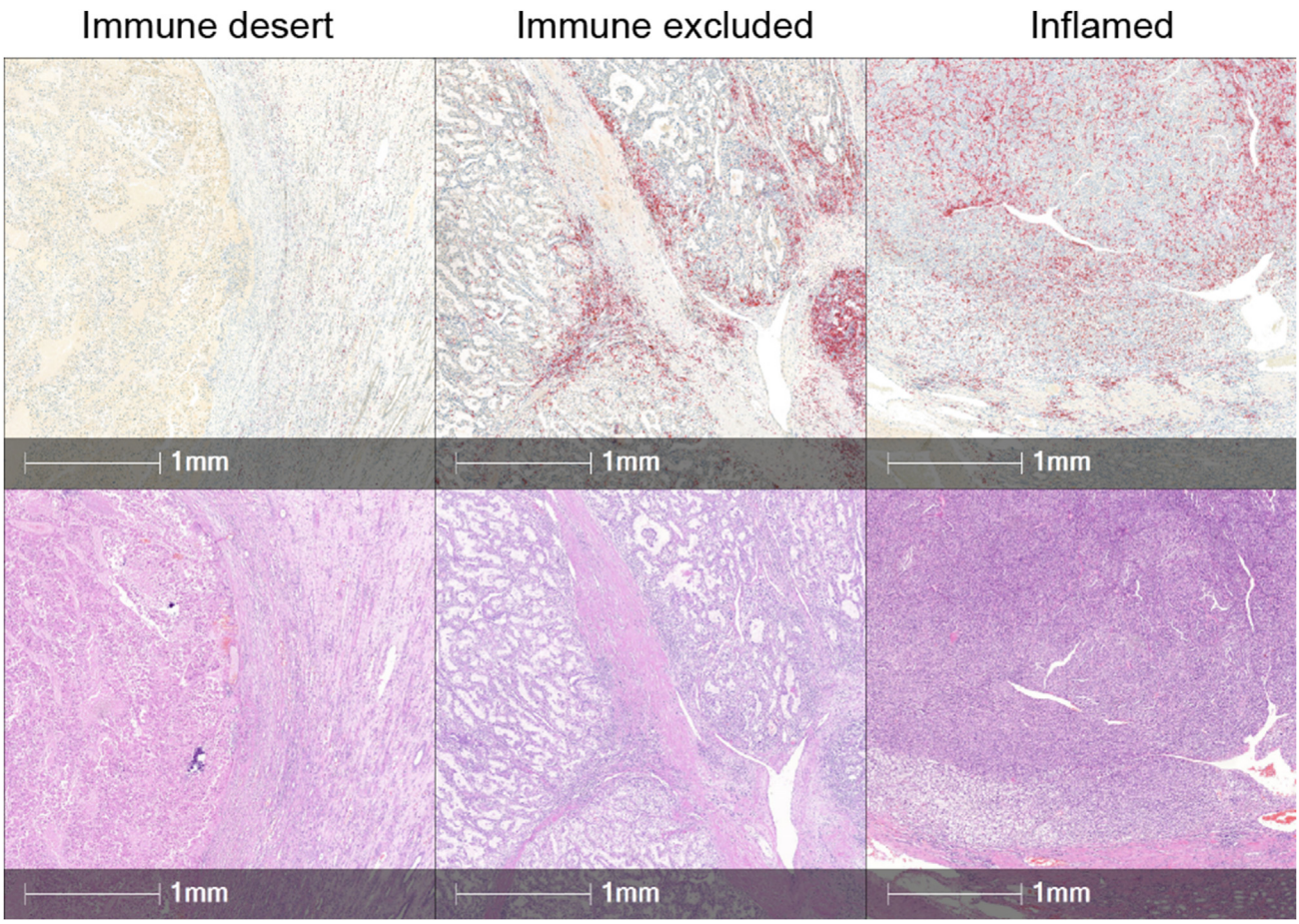

Figure 2.
Immune phenotypes. Overviews of $CD8^+$ T cells distribution within clear cell renal cell carcinoma as visualized by immunohistochemistry (upper row; CD8 in red) and the corresponding H&E (lower row). Tumors devoid (left) of $CD8^+$ T cells were termed immune desert. If $CD8^+$ T cells had arrived at the tumor bed but predominantly remained at the invasive margin or intratumoral stromal compartment, tumors were regarded as immune excluded (middle). Once $CD8^+$ T cells could be observed within the intratumoral compartment tumors were categorized as inflamed (right).

priming, we annotated TLS and accurately measured their size and frequency (Fig. 3D).

As expected, measured $CD8^+$ T-cell densities were significantly lower in tumors classified as immune desert or excluded than in inflamed PTs ($P < .0001$) and METs ($P < .0001$) (Tables 2). Inflamed/"hot" PTs with high infiltration densities of $CD8^+$ T cells showed a decreased DFS when compared with "cold" PTs, with the worst DFS for patients with inflamed/"hot" PTs containing high levels of exhausted $CD8^+TOX^+$ T cells (Supplementary Fig. S2).

Interestingly, the relative amount of $CD8^+TOX^+$ T cells was significantly increased in inflamed METs when compared with inflamed PTs ($P < .05$) yet without significant differences in the absolute overall $CD8^+$ T-cell densities (Fig. 3E). Intratumoral TLS (Fig. 3F) showed increased accumulative size in inflamed METs when compared with inflamed PTs ($P < .001$) (Supplementary Fig. S3).

Frameshift Mutations Occur as the Most Common Mutation Type

To evaluate the spectrum of molecular alterations between PTs and matched METs, we performed comprehensive targeted NGS analysis including the determination of the microsatellite status, the tumor mutational burden, and LOH. As expected, the majority of PTs showed mutations in *VHL* ($n = 38$, 80%), *PBRM1* ($n = 25$, 53%), and *SETD2* ($n = 14$, 30%) with 5 PTs carrying comutations in *VHL*, *PBRM1*, and *SETD1* (Fig. 1; Supplementary Fig. S4A).

All tumors displayed additional pathogenic mutations, interpreted as passenger mutations and various mutations of unknown significance (Supplementary Table S2). The 9 *VHL* wild-type PTs showed pathogenic mutations in *PBRM1* or *SETD2*, except for 2 cases that were triple wild-type (*VHL*, *PBRM1*, and *SETD2* wild-type) carrying mutations among others in *TP53* or *TERT*, respectively. Of the total number of potentially pathogenic mutations ($n = 340$), the large majority were frameshift mutations ($n = 139$), followed by missense mutations ($n = 56$), nonsense mutations ($n = 54$), mutations in splice sites ($n = 34$), homozygous losses ($n = 23$), amplifications ($n = 19$), deletions ($n = 7$), promoter mutations in *TERT* ($n = 5$), and rearrangements ($n = 3$) (Supplementary Fig. S4B and data not shown). Interestingly, 21% of cases showed genes exclusively mutated in the PTs that could not be detected in their matched distant metastasis (Supplementary Fig. S4C). Of these, *SETD2* and *PBRM1* were most frequent, showing isolated orphan mutations in *SETD2*, an isolated orphan mutation in *PBRM1*, and a cooccurrence of *SETD2* and *PBRM1* exclusively in the PT. In 1 case, both PT and the matched MET carried mutations in *VHL* but at different positions (PT: *VHL*

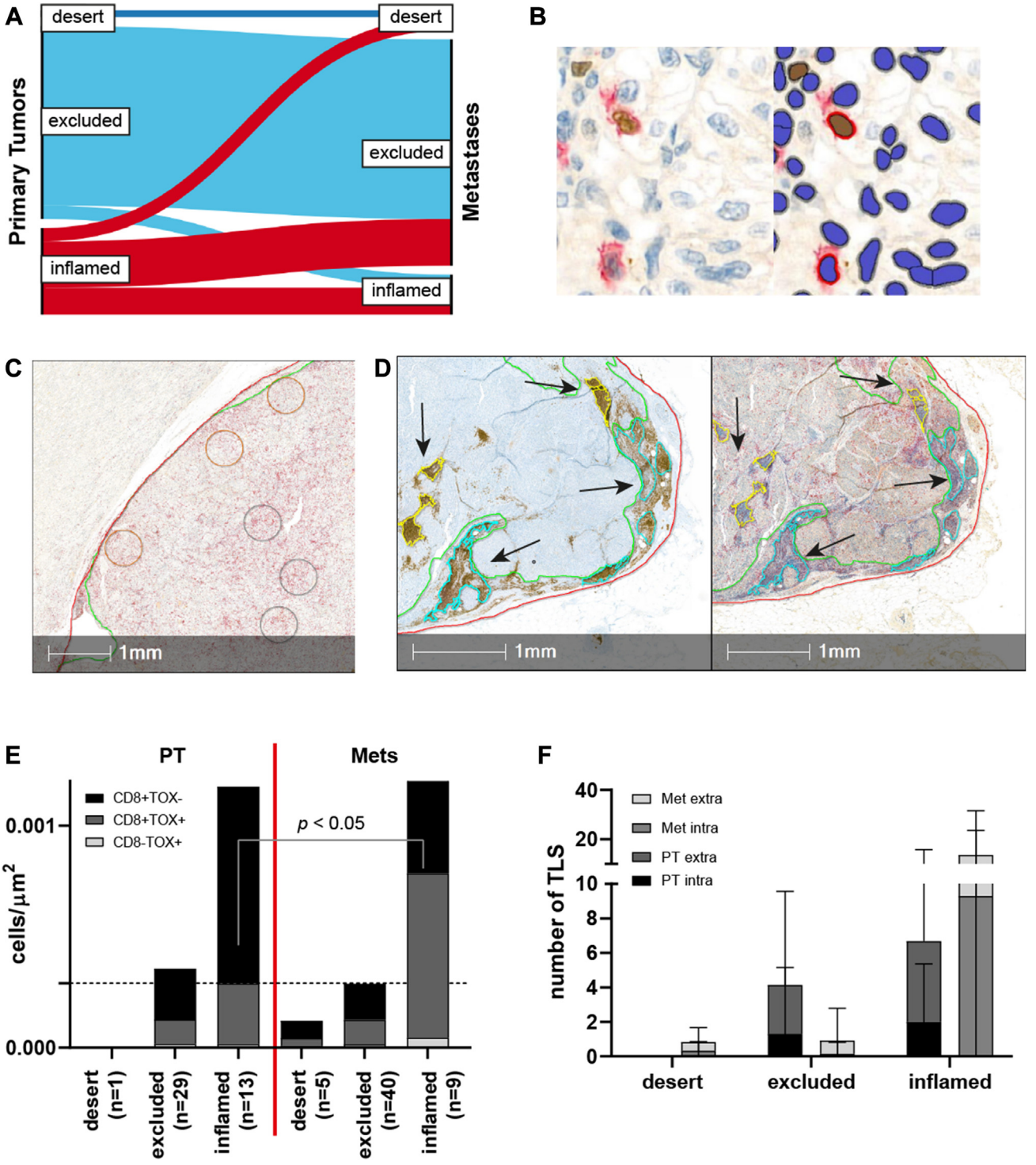

Figure 3.

Immune phenotypes, tumor-infiltrating CD8/TOX T cells and prevalence of tertiary lymphoid structures (TLS). Most clear cell renal cell carcinoma primary tumors (A, left) (desert = dark blue, excluded = blue, and inflamed = red) turned cold, and only a few remained inflamed at their metastatic site (A, right categories metastases). Whole slides were costained for CD8 (red) and TOX (brown) (B, left), revealing CD8+TOX−, CD8+TOX+, and CD8−TOX+ immune cells as further highlighted by the mark-up of the staining (B, right). For further analysis, virtual tissue microarrays were annotated from the tumor center (gray circles) and invasive margin (orange circles) compartment (C). TLS were defined as dense lymphocyte aggregate containing clusters of CD20+ B cells, measured within the tumor (termed TLS intra, yellow; within the tumor region, green) and within the extratumoral stroma but outside of the tumor (termed TLS extra, blue; within the extratumoral stroma, red). The left panel shows a CD20-stain (brown), the right panel the CD8 (red) and TOX (brown) stain of the same region (D). Although the absolute densities of intratumoral CD8/TOX immune cells and frequencies of TLS between the immune diagnostic categories remained similar between primary tumors and METs, distant METs showed a significant relative increase of intratumoral CD8+TOX+ T cells (E) and a tendency toward an increased frequency of intratumoral TLS (F).

Table 2
CD8+ Tox− T cells are significantly more prevalent in inflamed than in excluded or desert tumors both in primary tumors

Mean cells/μm²	Primary tumors		
	Desert ($n = 1$)	Excluded ($n = 29$)	Inflamed ($n = 13$)
$CD8^+$ Tox^-	0	0.0002	0.001
$CD8^+$ Tox^+	0	0.0001	0.0002
$CD8^-Tox^+$	0	0.00002	0.00001
Mean cells/μm²	Metastases		
	Desert ($n = 5$)	Excluded ($n = 40$)	Inflamed ($n = 9$)
$CD8^+$ Tox^-	0.00009	0.0002	0.001
$CD8^+$ Tox^+	0.00004	0.0001	0.001
$CD8^-Tox^+$	0.00001	0.00002	0.00003
P values	Primary tumors		
	Desert vs excluded	Desert vs inflamed	Excluded vs inflamed
$CD8^+$ Tox^-	ns	<.05	<.0001
$CD8^+$ Tox^+	ns	ns	ns
$CD8^-Tox^+$	ns	ns	ns
P values	Metastases		
	Desert vs excluded	Desert vs inflamed	Excluded vs inflamed
$CD8^+$ Tox^-	n.s.	<.05	<.0001
$CD8^+$ Tox^+	ns	<.001	<.0001
$CD8^-Tox^+$	n.s.	ns	ns
P values	PT vs Metastases		
	Desert	Excluded	Inflamed
$CD8^+$ Tox^-	ns	ns	ns
$CD8^+$ Tox^+	ns	ns	<.05
$CD8^-Tox^+$	ns	ns	ns

CD8+ Tox− T cells represent the predominant population in comparison to CD8+ Tox+ T cells and CD8− Tox+ cells regardless of the immune phenotype in the primary tumors. In contrast, CD8+ Tox+ T cells significantly increase at the metastatic sites.
ns, nonsignificant; PT, primary tumors.

D179fs*23, MET: *VHL* splice site 340+2T>A). Of all frequently mutated genes in PT, *SETD2,* and *PBRM1* were more commonly lost in the matched METs (Supplementary Fig. S4C). Remarkably, orphan mutations of both genes were also detected in isolation within the matched METs (*SETD2, n* = 9 and *PBRM1, n* = 5), which were *SETD2* and *PBRM1* wild-type in their corresponding PTs (Supplementary Fig. S4D). These observations were irrespective of the location of metastatic site or the time difference between sampling of the PT and the MET (data not shown). The tumor mutational burden was generally low (<10 mutations/Mb; data not shown), and both PT and METs were microsatellite stable (data not shown). In contrast to their PTs, matched METs showed more frequent copy number alterations but with similar patterns of LOH and large-scale state transition scores (data not shown). To confirm the copy number results of the targeted panel, we performed additional whole-genome-wide single nucleotide polymorphism-based array analysis for a subset of cases ($n = 14$). The genome-wide analysis similarly showed losses, particularly at chromosome 3p and gains at chromosome 5q without major differences between PTs and matched metastases (Supplementary Fig. S5). In consideration of the NGS and single nucleotide polymorphism array results, the De Novo occurrence of homologous-recombination deficiency in the metastases appeared unlikely.

Table 3
Genotype-immune phenotype associations

Gene	"Cold" ($n = 73$)	"Hot" ($n = 20$)	*P* value (Fisher exact test)
CDKN2A			.0015
Wild-type	72	15	
Mutated	1	5	
CDKN2B			.0071
Wild-type	72	16	
Mutated	1	4	
MTAP			.0302
Wild-type	72	17	
Mutated	1	3	
BAP1			.0071
Wild-type	72	16	
Mutated	1	4	

On the basis of a single gene analysis, inflamed tumors were associated with losses in BAP1, CDKN2A/B and MTAP when performing Fisher's exact tests.

Loss of BAP1, CDKN2A/B, and MTAP Is Associated With an Inflamed Immune Phenotype

To identify potential genotype-immune phenotype associations, we performed an integrative analysis with particular focus on genes reported to be commonly altered in either inflamed (*BAP1* and *CDKN2A/B*) or poorly immunogenic (*PBRM1* and *KDM5C*) ccRCC.[41] The association analysis was tailored on both single and multiple gene modes on the combined sets of PT and MET. The single gene analysis identified significantly more frequent loss-of-function mutations of *BAP1*, *CDKN2A/B,* and *MTAP* in tumors described as inflamed (Table 3).

However, we could not detect any significant association between *PBRM1* and *KDM5C*. Next, we overlaid the corresponding reactome pathways and examined whether any of the pathways is associated with the immune phenotype. The results revealed interleukin-12 signaling enrichment in inflamed ccRCC (gene set: MTAP/JAK2; $P = .007$) consistent with a proinflammatory milieu (Supplementary Table S3).

Discussion

The functional impact of genetic alterations on the TIME is complex, most likely context-dependent and incompletely understood, especially at metastatic sites.[42,43] Considering the polyclonal nature of cancer[44] and the effects of clinical therapies on tumor genetics and/or its immune landscape,[45] investigation of metastases seems essential to uncover actionable targets and understand disease progression and drug response. Our study provides insight into differences in the tumor immune infiltrates and tumor-intrinsic genetic alterations between primary ccRCC and matched distant metastases.

Seven distinct evolutionary subtypes of ccRCC have been suggested based on spatially separated whole-exome sequencing analysis of primary tumor ccRCC.[46] For most patients, driver events such as loss-of-function mutation in VHL could be detected in the PT and matched METs. In some instances, additional mutations in PBRM1 and/or SETD2 were exclusively identified at the metastatic site, indicating potential subclonal events in the primary tumors that went undetected. Alternatively, these mutations might have emerged De Novo within the metastasis, highlighting the spatiotemporal heterogeneity, especially given the 0 to 17-year time gap between primary tumor removal and metastasis resection observed in the current study.[14]

Associations of established predictive biomarkers linked to tumor inflammation such as increased tumor mutational burden or microsatellite instability[25] were not found in our cohort. Neither could we observe any association between the increased frequencies of frameshift mutations[47,48] with any particular immune phenotype. Despite the rather small cohort size, loss of *BAP1* and *CDKN2A/B* was associated with inflamed tumors as suggested previously, yet spatial CD8+ T-cell assessment has not been previously reported.[41,49,50] In PTs, increased amounts of $CD8^+$ T cells within the tumor center compartment of the PT correlated with an overall decreased DFS, with the worst DFS for PTs showing high densities of $CD8^+$ TOX^+ T cells. In view of these findings and the controversial predictive and prognostic role of tumor-infiltrating $CD8^+$ T cells in ccRCC,[16,19,51,52] prospective clinical trials employing ICI and utilizing digital image analysis are required to decipher the role of tumor-infiltrating CD8+ T cells in ccRCC. Overall, we observed a higher frequency of immune excluded or immune desert lesions in METs compared with PTs corresponding to clinically "cold" tumors as described in other malignancies.[40,53] Interestingly, the relative amount of $CD8^+TOX^+$ T cells of all $CD8^+$ T cells was increased within inflamed METs, suggesting a preceding antitumor immunity[54] and potentially tumor-experienced $CD8^+$ T cells. Whether this relative increase in $CD8^+TOX^+$ T cells in METs is associated with decreased survival also in the PTs needs to be determined.

Why metastatic sites commonly turn "cold" remains largely unknown. Genetic alterations, such as the observed *PBRM1* and *SETD2* mutations in METs, could amplify *STAT3* transcription[55] and methylate STAT1, respectively,[56] which in turn may cause expression of immune checkpoints and, as such, lead to T-cell exhaustion.[57] This potential impact on signal transducer and activator of transcriptions could be a possible explanation for our observed "cold" METs with an increase in exhausted $CD8^+$ T cells. In contrast, the impact of chromosomal instability (CIN) on antitumor immunity is less investigated. Cutoff values defining categories like "low," "intermediate," or "high" CIN tumors are not available, and comparative studies are lacking to this point. CIN, however, seems to influence antitumor immunity in a context-dependent fashion.[44] It may promote inflammation and tumor cell eradication by supporting tumor heterogeneity with expression of a larger panel of tumor antigens,[58-60] or it may support tumor immune evasion through chromosomal instability-mediated depletion of neoantigens resulting in the development of less immunogenic metastases. In our cohort, copy number alterations were not associated with an immune phenotype, neither in PTs nor METs, but we cannot exclude other types of chromosomal instability mechanisms like translocations exerting an impact on the immune infiltrates.

Our study has inherent shortcomings related to the number of samples and treatment heterogeneity. Well-characterized cohorts of PTs and matched metastatic lesions are rare, as they demand a large archive of tissue. Metastatic tissue is often monitored by imaging only or biopsied for confirmation. The limited tissue availability of METs thus hampers the compilation of such cohorts. Nevertheless, we identified genotype-immune phenotype associations in ccRCC that support an important and central role of *BAP1* and *CDKN2A/B* deficiency in ccRCC tumor inflammation. Although there is significant similarity in genetic mutations and the general immune presence within both PTs and their matched METs, our findings support investigation of METs because of the observed differences in immune infiltration and genetic profiles, calling for further investigation on the complex genetic and immune landscape in nonmetastatic vs metastatic disease. The integration of multimodal data sets like comprehensive molecular genotyping with spatially resolved tissue microenvironment analysis may help better understand genotype-immune phenotype associations, may uncover actionable targets, and may support our understanding of disease progression and drug response.

Acknowledgments

The authors would like to thank Juergen Hench from the Institute of Medical Genetics and Pathology, University Hospital Basel, Basel, Switzerland for exceptional support regarding the EpicArray data interpretation, and Susanne Dettwiler and Fabiola Prutek from the Department of Pathology and Molecular Pathology, University Hospital Zurich for outstanding tissue management and technical assistance.

Author Contributions

B.S., V.H.K., and H.M. conceptualized the study. B.S., V.V., and V.H.K. performed pathology review, reviewed and guided annotation work, performed data analysis and wrote the manuscript. A.L., K.D.M., M.B., and L.d.L. gave important intellectual input and provided samples. A.S. and D.B. helped retrieve clinical information. M.N. performed slide scanning and quality control, annotated scanned images, provided intellectual input and performed image analysis. A.K. and A.B.-E. performed data analysis of FoundationOne CDx and of EPIC array results. All authors discussed the included results and contributed to the final manuscript.

Data Availability

The datasets generated during and/or analyzed during the current study are available from the corresponding author upon reasonable request and institutional data governance board approval.

Funding

H.M. and L.d.L. were supported by the Swiss National Science Foundation, Switzerland (PathoLink Project 31BL30_172718). V.H.K. gratefully acknowledges funding by the Promedica Foundation F-87701-41-01.

Declaration of Competing Interest

None declared.

Ethics Approval and Consent to Participate

The study was approved by the ethics committee of the canton of Zurich (BASEC: 2018-02282) and a written informed consent was obtained from all patients prior to participation in this study.

Supplementary Material

The online version contains supplementary material available at https://doi.org/10.1016/j.modpat.2024.100558

References

1. Hsieh JJ, Purdue MP, Signoretti S, et al. Renal cell carcinoma. *Nat Rev Dis Primers*. 2017;3:17009. https://doi.org/10.1038/nrdp.2017.9
2. McDermott DF, Sosman JA, Sznol M, et al. Atezolizumab, an anti-programmed death-ligand 1 antibody, in metastatic renal cell carcinoma: long-term safety, clinical activity, and immune correlates from a phase Ia study. *J Clin Oncol*. 2016;34(8):833–842. https://doi.org/10.1200/JCO.2015.63.7421
3. Motzer RJ, Penkov K, Haanen J, et al. Avelumab plus axitinib versus sunitinib for advanced renal-cell carcinoma. *N Engl J Med*. 2019;380(12):1103–1115. https://doi.org/10.1056/NEJMoa1816047
4. Albiges L, Powles T, Staehler M, et al. Updated European Association of Urology guidelines on renal cell carcinoma: immune checkpoint inhibition is the new backbone in first-line treatment of metastatic clear-cell renal cell carcinoma. *Eur Urol*. 2019;76(2):151–156. https://doi.org/10.1016/j.eururo.2019.05.022
5. Binnewies M, Roberts EW, Kersten K, et al. Understanding the tumor immune microenvironment (TIME) for effective therapy. *Nat Med*. 2018;24(5):541–550. https://doi.org/10.1038/s41591-018-0014-x
6. Linehan WM, Ricketts CJ. The Cancer Genome Atlas of renal cell carcinoma: findings and clinical implications. *Nat Rev Urol*. 2019;16(9):539–552. https://doi.org/10.1038/s41585-019-0211-5
7. Peña-Llopis S, Vega-Rubín-de-Celis S, Liao A, et al. BAP1 loss defines a new class of renal cell carcinoma. *Nat Genet*. 2012;44(7):751–759. https://doi.org/10.1038/ng.2323
8. Cancer Genome Atlas Research Network. Comprehensive molecular characterization of clear cell renal cell carcinoma. *Nature*. 2013;499(7456):43–49. https://doi.org/10.1038/nature12222
9. Hakimi AA, Ostrovnaya I, Reva B, et al. Adverse outcomes in clear cell renal cell carcinoma with mutations of 3p21 epigenetic regulators BAP1 and SETD2: a report by MSKCC and the KIRC TCGA research network. *Clin Cancer Res*. 2013;19(12):3259–3267. https://doi.org/10.1158/1078-0432.CCR-12-3886
10. Wang T, Lu R, Kapur P, et al. An empirical approach leveraging tumorgrafts to dissect the tumor microenvironment in renal cell carcinoma identifies missing link to prognostic inflammatory factors. *Cancer Discov*. 2018;8(9):1142–1155. https://doi.org/10.1158/2159-8290.CD-17-1246
11. Motzer RJ, Banchereau R, Hamidi H, et al. Molecular subsets in renal cancer determine outcome to checkpoint and angiogenesis blockade. *Cancer Cell*. 2020;38(6):803–817.e4. https://doi.org/10.1016/j.ccell.2020.10.011
12. Gu Y-F, Cohn S, Christie A, et al. Modeling renal cell carcinoma in mice: Bap1 and Pbrm1 inactivation drive tumor grade. *Cancer Discov*. 2017;7(8):900–917. https://doi.org/10.1158/2159-8290.CD-17-0292
13. Kapur P, Peñna-Llopis S, Christie A, et al. Effects on survival of BAP1 and PBRM1 mutations in sporadic clear-cell renal-cell carcinoma: a retrospective analysis with independent validation. *Lancet Oncol*. 2013;14(2):159–167. https://doi.org/10.1016/S1470-2045(12)70584-3
14. Turajlic S, Xu H, Litchfield K, et al. Tracking cancer evolution reveals constrained routes to metastases: TRACERx renal. *Cell*. 2018;173(3):581–594.e12. https://doi.org/10.1016/j.cell.2018.03.057
15. Gerlinger M, Rowan AJ, Horswell S, et al. Intratumor heterogeneity and branched evolution revealed by multiregion sequencing. *N Engl J Med*. 2012;366(10):883–892. https://doi.org/10.1056/NEJMoa1113205
16. Nakano O, Sato M, Naito Y, et al. Proliferative activity of intratumoral CD8(+) T-lymphocytes as a prognostic factor in human renal cell carcinoma: clinicopathologic demonstration of antitumor immunity. *Cancer Res*. 2001;61(13):5132–5136.
17. Bromwich EJ, McArdle PA, Canna K, et al. The relationship between T-lymphocyte infiltration, stage, tumour grade and survival in patients undergoing curative surgery for renal cell cancer. *Br J Cancer*. 2003;89(10):1906–1908. https://doi.org/10.1038/sj.bjc.6601400
18. Siddiqui SA, Frigola X, Bonne-Annee S, et al. Tumor-infiltrating Foxp3-CD4+CD25+ T cells predict poor survival in renal cell carcinoma. *Clin Cancer Res*. 2007;13(7):2075–2081. https://doi.org/10.1158/1078-0432.CCR-06-2139
19. Granier C, Dariane C, Combe P, et al. Tim-3 expression on tumor-infiltrating PD-1^{+}CD8^{+} T cells correlates with poor clinical outcome in renal cell carcinoma. *Cancer Res*. 2017;77(5):1075–1082. https://doi.org/10.1158/0008-5472.CAN-16-0274
20. Hotta K, Sho M, Fujimoto K, et al. Prognostic significance of CD45RO+ memory T cells in renal cell carcinoma. *Br J Cancer*. 2011;105(8):1191–1196. https://doi.org/10.1038/bjc.2011.368
21. Jensen HK, Donskov F, Nordsmark M, Marcussen N, von der Maase H. Increased intratumoral FOXP3-positive regulatory immune cells during interleukin-2 treatment in metastatic renal cell carcinoma. *Clin Cancer Res*. 2009;15(3):1052–1058. https://doi.org/10.1158/1078-0432.CCR-08-1296
22. Giraldo NA, Becht E, Pagès F, et al. Orchestration and prognostic significance of immune checkpoints in the microenvironment of primary and metastatic renal cell cancer. *Clin Cancer Res*. 2015;21(13):3031–3040. https://doi.org/10.1158/1078-0432.CCR-14-2926
23. Baine MK, Turcu G, Zito CR, et al. Characterization of tumor infiltrating lymphocytes in paired primary and metastatic renal cell carcinoma specimens. *Oncotarget*. 2015;6(28):24990–25002. https://doi.org/10.18632/oncotarget.4572
24. Rooney MS, Shukla SA, Wu CJ, Getz G, Hacohen N. Molecular and genetic properties of tumors associated with local immune cytolytic activity. *Cell*. 2015;160(1-2):48–61. https://doi.org/10.1016/j.cell.2014.12.033
25. Thorsson V, Gibbs DL, Brown SD, et al. The immune landscape of cancer. *Immunity*. 2018;48(4):812–830.e14. https://doi.org/10.1016/j.immuni.2018.03.023
26. Herbst RS, Soria J-C, Kowanetz M, et al. Predictive correlates of response to the anti-PD-L1 antibody MPDL3280A in cancer patients. *Nature*. 2014;515(7528):563–567. https://doi.org/10.1038/nature14011
27. Waldman AD, Fritz JM, Lenardo MJ. A guide to cancer immunotherapy: from T cell basic science to clinical practice. *Nat Rev Immunol*. 2020;20(11):651–668. https://doi.org/10.1038/s41577-020-0306-5
28. Hegde PS, Karanikas V, Evers S. The where, the when, and the how of immune monitoring for cancer immunotherapies in the era of checkpoint inhibition. *Clin Cancer Res*. 2016;22(8):1865–1874. https://doi.org/10.1158/1078-0432.CCR-15-1507
29. Sobottka B, Nowak M, Frei AL, et al. Establishing standardized immune phenotyping of metastatic melanoma by digital pathology. *Lab Invest*. 2021;101(12):1561–1570. https://doi.org/10.1038/s41374-021-00653-y
30. Sobottka B, Nienhold R, Nowak M, et al. Integrated analysis of immunotherapy treated clear cell renal cell carcinomas: an exploratory study. *J Immunother*. 2022;45(1):35–42. https://doi.org/10.1097/CJI.0000000000000387
31. Horeweg N, de Bruyn M, Nout RA, et al. Prognostic integrated image-based immune and molecular profiling in early-stage endometrial cancer. *Cancer Immunol Res*. 2020;8(12):1508–1519. https://doi.org/10.1158/2326-6066.CIR-20-0149
32. Wang X, He Q, Shen H, et al. TOX promotes the exhaustion of antitumor CD8^{+} T cells by preventing PD1 degradation in hepatocellular carcinoma. *J Hepatol*. 2019;71(4):731–741. https://doi.org/10.1016/j.jhep.2019.05.015
33. Kim K, Park S, Park SY, et al. Single-cell transcriptome analysis reveals TOX as a promoting factor for T cell exhaustion and a predictor for anti-PD-1 responses in human cancer. *Genome Med*. 2020;12(1):22. https://doi.org/10.1186/s13073-020-00722-9
34. Braun DA, Street K, Burke KP, et al. Progressive immune dysfunction with advancing disease stage in renal cell carcinoma. *Cancer Cell*. 2021;39(5):632–648.e8. https://doi.org/10.1016/j.ccell.2021.02.013
35. Li R, Ferdinand JR, Loudon KW, et al. Mapping single-cell transcriptomes in the intra-tumoral and associated territories of kidney cancer. *Cancer Cell*. 2022;40(12):1583–1599.e10. https://doi.org/10.1016/j.ccell.2022.11.001
36. Lawrence M, Huber W, Pagès H, et al. Software for computing and annotating genomic ranges. *PLoS Comput Biol*. 2013;9(8):e1003118. https://doi.org/10.1371/journal.pcbi.1003118
37. Aryee MJ, Jaffe AE, Corrada-Bravo H, et al. Minfi: a flexible and comprehensive Bioconductor package for the analysis of Infinium DNA methylation microarrays. *Bioinformatics*. 2014;30(10):1363–1369. https://doi.org/10.1093/bioinformatics/btu049
38. Amgad M, Stovgaard ES, Balslev E, et al. Report on computational assessment of tumor infiltrating lymphocytes from the International Immuno-Oncology Biomarker Working Group. *NPJ Breast Cancer*. 2020;6(1):16. https://doi.org/10.1038/s41523-020-0154-2
39. Quintayo MA, Starczynski J, Yan FJ, et al. Virtual tissue microarrays: a novel and viable approach to optimizing tissue microarrays for biomarker research applied to ductal carcinoma in situ. *Histopathology*. 2014;65(1):2–8. https://doi.org/10.1111/his.12336
40. Sobottka B, Moch H, Varga Z. Differential PD-1/LAG-3 expression and immune phenotypes in metastatic sites of breast cancer. *Breast Cancer Res*. 2021;23(1):4. https://doi.org/10.1186/s13058-020-01380-w
41. Brugarolas J, Rajaram S, Christie A, Kapur P. The evolution of angiogenic and inflamed tumors: the renal cancer paradigm. *Cancer Cell*. 2020;38(6):771–773. https://doi.org/10.1016/j.ccell.2020.10.021
42. Huang Y, Gao S, Wu S, et al. Multilayered molecular profiling supported the monoclonal origin of metastatic renal cell carcinoma. *Int J Cancer*. 2014;135(1):78–87. https://doi.org/10.1002/ijc.28654
43. Serie DJ, Joseph RW, Cheville JC, et al. Clear cell type A and B molecular subtypes in metastatic clear cell renal cell carcinoma: tumor heterogeneity and aggressiveness. *Eur Urol*. 2017;71(6):979–985. https://doi.org/10.1016/j.eururo.2016.11.018
44. Tijhuis AE, Johnson SC, McClelland SE. The emerging links between chromosomal instability (CIN), metastasis, inflammation and tumour immunity. *Mol Cytogenet*. 2019;12:17. https://doi.org/10.1186/s13039-019-0429-1
45. Bi K, He MX, Bakouny Z, et al. Tumor and immune reprogramming during immunotherapy in advanced renal cell carcinoma. *Cancer Cell*. 2021;39(5):649–661.e5. https://doi.org/10.1016/j.ccell.2021.02.015
46. Turajlic S, Xu H, Litchfield K, et al. Deterministic evolutionary trajectories influence primary tumor growth: TRACERx renal. *Cell*. 2018;173(3):595–610.e11. https://doi.org/10.1016/j.cell.2018.03.043
47. Turajlic S, Litchfield K, Xu H, et al. Insertion-and-deletion-derived tumour-specific neoantigens and the immunogenic phenotype: a pan-cancer

analysis. *Lancet Oncol*. 2017;18(8):1009–1021. https://doi.org/10.1016/S1470-2045(17)30516-8
48. Hansen UK, Ramskov S, Bjerregaard A-M, et al. Tumor-infiltrating T cells from clear cell renal cell carcinoma patients recognize neoepitopes derived from point and frameshift mutations. *Front Immunol*. 2020;11:373. https://doi.org/10.3389/fimmu.2020.00373
49. Zhou Q, Qi Y, Wang Z, et al. CCR5 blockade inflames antitumor immunity in BAP1-mutant clear cell renal cell carcinoma. *J Immunother Cancer*. 2020;8(1):e000228. https://doi.org/10.1136/jitc-2019-000228
50. Shrestha R, Nabavi N, Lin Y-Y, et al. BAP1 haploinsufficiency predicts a distinct immunogenic class of malignant peritoneal mesothelioma. *Genome Med*. 2019;11(1):8. https://doi.org/10.1186/s13073-019-0620-3
51. Giraldo NA, Becht E, Vano Y, et al. Tumor-infiltrating and peripheral blood T-cell immunophenotypes predict early relapse in localized clear cell renal cell carcinoma. *Clin Cancer Res*. 2017;23(15):4416–4428. https://doi.org/10.1158/1078-0432.CCR-16-2848
52. Davis D, Tretiakova MS, Kizzar C, et al. Abundant CD8+ tumor infiltrating lymphocytes and beta-2-microglobulin are associated with better outcome and response to interleukin-2 therapy in advanced stage clear cell renal cell carcinoma. *Ann Diagn Pathol*. 2020;47:151537. https://doi.org/10.1016/j.anndiagpath.2020.151537
53. Sobottka B, Pestalozzi B, Fink D, Moch H, Varga Z. Similar lymphocytic infiltration pattern in primary breast cancer and their corresponding distant metastases. *Oncoimmunology*. 2016;5(6):e1153208. https://doi.org/10.1080/2162402X.2016.1153208
54. Helmink BA, Reddy SM, Gao J, et al. B cells and tertiary lymphoid structures promote immunotherapy response. *Nature*. 2020;577(7791):549–555. https://doi.org/10.1038/s41586-019-1922-8
55. Nargund AM, Pham CG, Dong Y, et al. The SWI/SNF protein PBRM1 restrains VHL-loss-driven clear cell renal cell carcinoma. *Cell Rep*. 2017;18(12):2893–2906. https://doi.org/10.1016/j.celrep.2017.02.074
56. Chen K, Liu J, Liu S, et al. Methyltransferase SETD2-mediated methylation of STAT1 is critical for interferon antiviral activity. *Cell*. 2017;170(3):492–506.e14. https://doi.org/10.1016/j.cell.2017.06.042
57. Benci JL, Xu B, Qiu Y, et al. Tumor interferon signaling regulates a multigenic resistance program to immune checkpoint blockade. *Cell*. 2016;167(6):1540–1554.e12. https://doi.org/10.1016/j.cell.2016.11.022
58. Senovilla L, Vitale I, Martins I, et al. An immunosurveillance mechanism controls cancer cell ploidy. *Science*. 2012;337(6102):1678–1684. https://doi.org/10.1126/science.1224922
59. Angelova M, Mlecnik B, Vasaturo A, et al. Evolution of metastases in space and time under immune selection. *Cell*. 2018;175(3):751–765.e16. https://doi.org/10.1016/j.cell.2018.09.018
60. Milo I, Bedora-Faure M, Garcia Z, et al. The immune system profoundly restricts intratumor genetic heterogeneity. *Sci Immunol*. 2018;3(29):eaat1435. https://doi.org/10.1126/sciimmunol.aat1435